Investigating Scour Impacts on Natural Frequency Changes and Sensitivity in Offshore Wind Turbine with Tripod Suction Bucket Foundations in Sand

Kyeong-Sun Kim[a], Seung-Won Oh[b], Beom-Soo Kim[c], Sung-Ryul Kim[d,*]

[a,b,c,d] *Department of Civil and Environmental Engineering, Seoul National University, 1 Gwanak-ro, Gwanak-gu, Seoul, South Korea*

Abstract

Scour-induced stiffness reduction affects the dynamic properties of offshore wind turbine foundations, but its impact on multi-footing structures is not fully elucidated. This study investigates the dynamic response of a 4.2 MW offshore wind turbine with a tripod suction bucket foundation under local scour conditions, employing geotechnical centrifuge experiments to model soil-structure interactions in sandy soil. Experiments on a scaled prototype model across varying scour depths demonstrated a consistent decrease in the first natural frequency, with a maximum 5.3% reduction at a scour depth of 60% of the bucket diameter. Contrary to monopiles, the multi-footing structural arrangement mitigates scour-induced stiffness degradation in a different manner, presumably through stress redistribution among the legs, as corroborated by variations in observed natural frequency sensitivities to scour. Finally, we developed a predictive model for natural frequency-based scour sensitivity considering foundation flexibility, which was thoroughly validated by comparing its predictions with the results obtained from the centrifuge tests.

Keywords: scour, offshore wind turbine, centrifuge test, tripod suction bucket foundation, natural frequency

1. Introduction

Offshore wind turbines (OWTs) require robust foundation systems to maintain structural integrity under complex loading conditions, including waves, currents, and wind. Among these external factors, seabed erosion—commonly referred to as scour—constitutes a critical threat to foundation stability. Scour removes sediment from around the foundation, effectively reducing the lateral soil support, and leads to a decrease in natural frequency (Zaaijer, 2006). This natural frequency drop is widely recognized as an indicator of scour-induced damage; the removal of supporting soil layers renders the structure more flexible, shifting its natural frequency closer to resonance with rotor or wave excitation frequencies, which could be detrimental.

A common structural health monitoring approach is to track these natural frequency shifts as a proxy for scour depth. Existing research has predominantly focused on monopile-supported OWTs, which are single large-diameter piles driven into the seabed, commonly used in shallower waters. Studies such as Sørensen & Ibsen (2013) and Van der Tempel et al. (2004) have demonstrated that increased scour depth reduces lateral support, thereby lowering natural frequencies. Similarly, Bhattacharya (2019) warned that scour can shift the tower's natural frequency into the 1P–3P

**Corresponding author.*

Email address: sungryul@snu.ac.kr (Sung-Ryul Kim)

Tel: +82-2-880-8760

rotor excitation range, potentially increasing the risk of failure if left unmitigated. Empirical data and numerical simulations have consistently shown that fully developed scour on monopiles in the range of one pile diameter can yield natural frequency drops on the order of 5–10% (Kallehave et al., 2015). Although these percentage shifts may appear moderate, they can critically reduce safety margins by bringing the structure closer to resonance.

While monopile foundations have been the focus of most scour-related research, the offshore wind industry is rapidly adopting alternative foundation systems – including suction bucket and multi-footing (e.g. tripod or tetrapod) designs – that demand similar scrutiny. Suction bucket foundations (large-diameter caissons installed by under-pressure) and multi-footing configurations offer attractive benefits such as cost-effective installation and high initial stiffness, and they have seen successful pilot applications in commercial projects (Houlsby, 2016). Notably, tripod jacket substructures with three suction buckets (one at each leg) have been deployed in European projects like the Borkum Riffgrund and Aberdeen offshore wind farms, as well as in Asia (e.g. Changle wind farm in China). These multi-footing foundations can provide greater resistance to lateral loads and overturning moments compared to a single large monopile, potentially resulting in a higher baseline natural frequency for the supported turbine.

Despite wide acceptance, studies for the multi-footing structures (e.g. tripod and tetrapod) have received less attention. Only in recent years an increasing number of centrifuge tests have aimed to explore the performance of multi-footing structures in more realistic scaled conditions. Kim et al. (2014) investigated monotonic and cyclic behavior of monopod and tripod bucket foundations for offshore wind towers using centrifuge modeling. Also, Jeong et al. (2019) conducted 70-g centrifuge tests on tripod suction bucket foundations, showing that failure is governed by rigid-body rotation involving passive soil resistance in front of the loaded buckets and tension (suction) in trailing buckets. These findings underscore the fundamental differences in load transfer mechanisms between different foundation types (e.g., tripod suction bucket foundations) and conventional monopiles, as the distributed support significantly alters the patterns of soil failure and stiffness degradation.

Moreover, the influence of scour on such multi-footing structures remains relatively under-examined. Much of the centrifuge-based research to date has focused on characterizing monotonic or cyclic capacity rather than documenting changes in natural frequency under progressive scour. Few studies have explicitly incorporated scour simulations due to the inherent difficulty of replicating scour phenomena at small scale (Qi et al., 2016; Li et al., 2024). Despite its difficulty, Kariyawasam (2020) and Futai et al. (2021) performed centrifuge tests to measure shifts in monopile natural frequency as a function of scour depth, whereas parallel work by Arany et al. (2016) and Ryu et al. (2020) developed analytical frameworks to estimate natural frequency of OWT considering foundation stiffness with embedment depths. However, experimental data capturing dynamic responses as scour develops—especially the variation of system's natural frequency with time—remain relatively scarce.

Although multi-footing structures, such as tripod or jacket systems, are argued to be less sensitive to scour-induced natural frequency changes than monopiles due to load distribution among legs (Zaaijer & Tempel, 2004; Ma et al., 2018; Liang et al., 2020; Skau et al., 2018; Jawalageri et al., 2022), there remains a key research gap: limited experimental evidence quantifying how local scour affects natural frequency sensitivity in these foundations, particularly under progressive scour depths in sandy soils. Numerical studies suggest differential reductions in natural frequency between monopile- and tripod-supported OWTs under scour, but they lack validation from scaled physical

model tests capturing dynamic responses, including potential asymmetries from uneven scour. This study addresses this gap through geotechnical centrifuge tests on a tripod suction bucket foundation, with the objectives to: (1) quantify scour effects on the system's natural frequency, (2) assess the viability of frequency-based metrics for structural health monitoring in multi-footing systems, and (3) develop and validate a predictive model for scour sensitivity considering foundation flexibility.

This study examines the scour sensitivity of offshore wind turbine tower supported by tripod suction bucket foundation through centrifuge model tests in sand. The introduction of local scour around the three-bucket foundation in the centrifuge tests provides a novel experimental quantification of stiffness and natural frequency degradation for this foundation type. The specific objectives are to determine how incremental scour (in terms of removal of sand around the buckets) affects the system's dynamic responses. This research aims to provide an experimentally grounded understanding of how multi-footing structures respond to incremental scour depth. By capturing key dynamic parameters such as natural frequency under different scour conditions, the study also assesses the viability of using frequency-based metrics as an indicator of foundation health for multi-footing systems. Frequency-based structural health monitoring has already been proposed by OWI-Lab for monopile-based OWTs (Weijtjens et al., 2016) and transmission towers (Bel-Hadj et al., 2024), where shifts in natural frequency serve as a diagnostic for foundation scour or damage. Data-driven predictive models require reliable metrics for advancing state-of-the-art applications in offshore geotechnical engineering (Stuyts & Suryasentana, 2023). Scour sensitivity would provide clearer insights into scour-induced natural frequnecy shifts to promote advancement in maintenance strategies, helping to prolong the operational lifespan of offshore wind energy infrastructure.

2. Prototype conditions

2.1. Tower and tripod suction bucket foundation

The centrifuge modeling replicates a prototype 4.2 MW offshore wind turbine (OWT) supported by a tripod suction bucket (TSB) foundation, deployed as part of a field demonstration of the All-In-One-Installation (AIOI) process using a multi-purpose mobile base (MMB), as documented by Ryu et al. (2022). Turbine specifications and tower dimensions are sourced from KEPRI (2021). The 4.2 MW turbine features a rotor diameter of 136 m, blade length of 66.5 m, and rated wind speed of 11.3 m/s. It operates at a rotational speed of 10 rpm in a three-bladed, upwind configuration with a hub height of 95 m, exhibiting cut-in and cut-out wind speeds of 3 m/s and 22 m/s, respectively. The rotor-nacelle assembly (RNA) mass totals M_{RNA} 338 t, comprising 169 t (nacelle), 110.5 t (rotor), and 58.5 t (blades). The tower, with mass M_{t}= 1213 t, has a variable diameter of 3.5–4.2 m and wall thickness of 17–45 mm, yielding a flexural rigidity EI = 1.72 10^{11} Nm^2 (Ryu et al., 2020). The tower length without scour, measured from the RNA reference point to the seabed, is L_0 = 126.8m (See Fig. 1). The TSB foundation comprises three suction buckets of diameter D = 8.0m, skirt length L_{f} = 9.3m, and wall thickness of 20mm, interconnected by structural bracings with center-to-center spacing of 20 m (half-spacing R =10 m) and main colmuns of 3.0-4.2m diameter over a length of 31.8 m. In idealized structural model, the foundation vertical stiffness is k_{v} is used for soil-strucutral interaction. Under scour of depth S alongside skirt embedment L_f, the foundation experiences differential push-pull

action, with compression C and tension T forces acting on the leading and trailing buckets, respectively. Figure 1 illustrates the prototype location, OWT supported by the TSB foundation, and structural idealization for dynamic analysis in Section 5. Table 1 summarizes prototype and scaled model parameters.

Figure 1. (a) Location of the prototype offshore wind turbine (OWT) in the southwestern sea of the Korean Peninsula; (b) Schematic of the OWT supported by tripod suction bucket (TSB) foundation; (c) Structural idealization for analytical modeling

Table 1. The prototype and model tower and foundation parameters

2.2. Environmental conditions

The environmental conditions for this 4.2 MW OWT prototype model were extracted from the final design report of the Southwest Sea 2.5 GW Offshore Wind Farm Demonstration Complex (KEPRI, 2016). According to KEPRI (2016), meteorological data were sourced from the HeMOSU weather mast, spanning 2011–2013. Extreme wind speeds were estimated using annual maximum series fitted to a Generalized Extreme Value (GEV) distribution, a standard method for extrapolating return periods beyond available data lengths with 95% confidence intervals. Here, return period was defined as the average time between exceedances of a given wind speed threshold. Short-term records are commonly extrapolated in offshore wind design to infer long-term extremes, with uncertainties mitigated by regional statistical models and validation against nearby long-term datasets (e.g., IEC 61400-3 standards). This approach aligns with engineering practice for site-specific assessments, ensuring conservative estimates for structural loading.

The wind speed distribution was characterized at a reference height of 97 m as follows: for a 1-year return period, the 10-min average wind speed V_n was 27.76 m/s, with a 3-s gust speed V_{eN} of 32.42 m/s and power-law exponent α = 0.0907; for a 50-year return period, V_n was 43.06 m/s, V_{eN} was 50.29 m/s, and α = 0.0669. Here, V_n denotes the 10-min average wind speed, V_{eN} the 3-s gust wind speed, and α the power-law exponent describing vertical wind shear.

To visualize the main wind direction, the wind occurrence rates, defined as the percentage of time winds blow from each sector, were quantified across 12 directional sectors (30° intervals). Figure 2 illustrates the data of wind occurrence rates at two reference heights as each radial bar represents a 30° sector.

Figure 2. Wind rose diagram showing wind direction occurrence rates (frequency of winds from each 30° sector, as a percentage of total observations in wind speed distribution) at two different heights

2.3. Soil stratigraphy

The prototype 4.2 MW OWT was installed in the demonstration site near the southwestern sea of the Korean Peninsula (water depth 13.6 m), which features a layered soil profile. As reportd by Seo et al. (2021), the site stratigraphy comprises three layers (Table 2): (1) an upper sand layer (0–2.5 m) classified as clean to silty sand; (2)

an underlying clay and silt layer (2.5–8.3 m) classified as silty clay of low plasticity; and (3) a lower sand layer (8.3–10.7 m) classified as silty sand. Key properties include dry unit weight γ_d, CPT cone tip resistance q_t, standardized penetration test blow count N_{60}, effective friction angle ϕ, small-strain shear modulus G_0, undrained shear strength s_u, and overconsolidation ratio OCR. Three CPT profiles derived from the KEPRI Report (KEPRI, 2015) were used to inform the centrifuge model design, though three layer was simplified as one layer in the centrifuge test. The homogeneous sand layer was modelled in the centrifuge testing to ensure replicability and the model's utility.

Table 2. Prototype soil conditions at the demonstration site reported by KEPRI (2020)

For the centrifuge tests the cohesive clay/silt layer was omitted to focus on scour in sandy conditions, using a single uniform sand layer. Properties were averaged from the prototype's three layers to 10.7 m depth (e.g., mean γ_d ~ 18.8 kN/m³, q_t ~ 3.2 MPa, N_{60} ~ 9.0, ϕ ~ 37 deg, G_0 ~ 35 MPa; classified as clean to silty sand per Robertson, 2009. This simplification assumes a homogeneous profile for scour effect quantification but may overestimate natural frequency reductions under scour, as the absent clay layer may provide additional damping and slightly different stiffness that could mitigate degradation in the real site. Future tests with layered profiles would reduce this error, enhancing centrifuge model fidelity to the prototype.

2.4 Field observations for scour

The spatial distribution and variability of scour, visualized using depth profile plots (Figure 3a) and a rose diagram (Figure 3b) to depict the directional distribution of maximum scour depths immediately around each bucket, were used to inform the observed scour extent, angle, and asymmetry for centrifuge modeling.

To characterize scour around the tripod foundation, bathymetric surveys of the prototype offshore wind turbine (OWT) were conducted using multi-beam sonar one year post-installation. Multi-beam bathymetry employs acoustic sonar technology to measure seabed depth with high spatial resolution, emitting multiple sound beams that reflect off the seafloor. Raw bathymetric data were transformed into physical coordinates via affine transformation, calibrated against known bucket center locations. The data were then interpolated onto a uniform grid using linear interpolation to enable detailed seabed topography visualization around the buckets. Radial depth profiles were extracted from each bucket center at 15° angular increments, within a 5 m radius to capture scour immediately adjacent to the bucket skirts. Scour depth S was quantified as the vertical deviation from the reference elevation.

The maximum scour depth was selected to fall within a reasonable range informed by site-specific observations and literature on similar offshore conditions. The reasonable maximum scour range was defined here as scour depths up to 0.6 times the bucket diameter ($S/D \leq 0.6$), where S denotes scour depth and D bucket diameter. This range was selected by considering the field measurements of 1.5–2.0 m after major storms at the demonstration site (KOWP, 2021) and reported values for large-diameter suction bucket foundations (Stroescu et al., 2016).

Figure 3. Bathymetric survey results from multi-beam sonar. (a) Radial depth profiles showing seabed depth (vertical distance from reference mean sea level to scoured seafloor); (b) Scour depth rose diagram illustrating average scour depth S immediately around each bucket, calculated from seabed depths of bathymetric data

3. Geotechnical centrifuge test program

3.1 Experiment program and test setup

The dynamic behavior (e.g. natural frequency) of offshore wind turbine foundations was investigated through geotechnical centrifuge testing, enabling accurate simulation of prototype-scale stress conditions and detailed analysis of soil-structure interactions specific to tripod suction bucket foundations. All centrifuge tests were conducted using the geotechnical beam centrifuge at the Korea Advanced Institute of Science and Technology (KAIST), featuring a 5.0 m radius and capable of reaching accelerations up to 100 g with a payload capacity of 2,400 kg (Kim et al., 2013). Key scaling relationships, derived through similitude laws based on dimensional analysis, are summarized in Table 3.

Table 3. Scaling relationships for centrifuge test (Kutter, 1992)

A series of 12 test cases was performed at 70 g (1:70 geometric scale), consistent with previous tripod foundation studies (Jeong et al., 2019). The tests comprised a 3 × 4 matrix, varying three soil conditions across four progressive scour depths, selected within a realistic range informed by field observations at the prototype demonstration site. Table 4 summarizes the test cases in prototype units, including design parameters such as scour depth S at each of the three buckets (#1, #2, #3, with mean value); soil type (SP for clean silica sand; SP-SM for silica sand with silt); D_r relative density; initial small-strain shear modulus G_0 which was inferred by correlating cone penetration tip resistance; mass of piezoelectric actuator assembly M_{RNA} (ton); tower height above mudline L_0; and tower bending stiffness EI. Structural parameters (M_{RNA}, L_0, EI) follow the prototype specifications detailed in section 2.1.

Table 4. Summary of centrifuge test cases with details of design parameters (in prototype units)

The OWT model featured a cylindrical tower (total height 1493 mm in model scale) mounted centrally on a tripod substructure with three suction buckets of 114 mm diameter (8.0 m in prototype) and 132 mm skirt length (9.3 m in prototype). An amplified piezoelectric actuator (APA) was mounted atop the tower to simulate the prototype rotor-nacelle assembly mass precisely. Figure 4 illustrates the experimental arrangement and instrumentation of the centrifuge test.

Figure 4. (a) Centrifuge test setup showing strongbox, model OWT, and instrumentation; (b) Close-up of piezoelectric assembly located on top of the tower.

The offshore wind turbine model with tripod suction bucket foundation was housed in a rectangular aluminum strongbox, providing sufficient space around the tripod to avoid boundary interference. To minimize wave reflections and boundary effects, a 10 mm thick Duxseal layer lined the strongbox walls. Testing began with the sand surface level to the bucket lids (representing no-scour conditions) to obtain baseline data at 70g. The centrifuge flight was then stopped and returned to 1g, and the soil surface was excabated by a special tool for scour hole. Local scour was simulated by sequentially removing sand around each bucket, replicating field-observed patterns.

The data acquisition system interfaced through a fiber-optic rotary joint at a 19.2 kHz sampling rate via a DAQ PXI-1045 system with 32 channels using CatmanEasy software, ensuring precise synchronization of dynamic load application and sensor recording. A dynamic load cell (DDE-250N) and accelerometer (A0) recorded applied dynamic loads and acceleration at piezoelectric assembly. Following Kariyawasam (2020), ADXL1003 series MEMS accelerometers (A1 at tower top, A2 at mid-height, A3 at tower base) provided high-bandwidth, low-noise measurements of vibration. Accelerometers were calibrated prior to testing using a 1g device at the facility. Linear strain gauges along the tower exterior (near tower base) measured bending moment responses via local strain amplitudes.

3.2 Model structure

A geometrically scaled model of the OWT structure was fabricated from stainless steel to replicate the prototype's tower and tripod frame. For its material, a thin stainless steel, ASTM-A240M (density ≈7850 kg/m³; Young's modulus E ≈ 210 GPa; yield strength ≈ 262 MPa), was chosen. Laser welding was employed at all joints to maintain structural integrity and minimize distortions, the considerations of which were important for thin tubular structural members. To accurately measure natural frequency changes, the model's bending stiffness and mass distributions were calculated to align with theoretical predictions. In particular, the tapered cross-section of the tower and equivalent flexural rigidity of tower-tripod (TP) were simplified following Jalbi et al. (2019). The diameter of equivalent tubular members was determined a priori, and the effective wall thickness was computed to achieve the target flexural rigidity. Fine adjustments to the lumped mass were carefully made so that the small-scale structure's natural frequency matched the target full-scale natural frequency when scaled up, following Bhattacharya (2019). Ultimately, the structural integrity of the scaling was verified by comparing the model's structural properties at 1 g with theoretical predictions for the prototype, confirming the fidelity of the scaled structural system with mass and bending stiffness modelled within acceptable error margins (Figure 5).

Figure 5. Measurement by strain gauges at different locations for model's bending stiffness estimation

The strain measurements from strain gauges positioned at 0°, 90°, 180°, and 270° around the tower's perimeter at the base were used to calculate the total bending strain using Euclidean norm:

$$\epsilon_b = \sqrt{\epsilon_x{}^2 + \epsilon_y{}^2}, \tag{20}$$

where $\epsilon_x = (\tilde{\epsilon}_{0^\circ} - \tilde{\epsilon}_{180^\circ})/2$ and $\epsilon_y = (\tilde{\epsilon}_{90^\circ} - \tilde{\epsilon}_{270^\circ})/2$. Here, $\tilde{d}$ denotes the mean. Then, the model's bending stiffness EI was calculated by:

$$EI = \frac{M_b y}{\epsilon_b} \tag{21}$$

where y is distance from the neutral axis within the cross-section; M_b is the bending moment calculated as $= F \times d$ where F is the force exerted by the known mass at a distance d from the tower's central axis.

3.3 Model ground preparation

A uniformly graded silica sand and silica sand with silt were selected for ground modelling to replicate prototype seabed conditions, since silica sand is well-documented, known for its consistency, and widely used in centrifuge testing globally. Careful sieve analyses with wet sieving were carried out for silica sand (No. 7) and silica sand with silt (No. 8), both exhibiting similar key geotechnical properties such as a specific gravity (G_s) of 2.65 and uniformity coefficient (C_u) less than 3 (Figure 6).

Figure 6. Grain size distribution curves for silica sand (No.7) and silica sand with silt (No.8)

The silica sand with silt (No. 8) was classified as poorly graded sand with silt with dual symbol (e.g., SP-SM) because of higher fine content (e.g., sieve #200 <0.075 mm) per USCS (fines 12%) and it had poor grading (high C_u) with lower median grain size (d_{50}) of 0.15 mm. This sand with silt (12% fine content), combined with a high uniformity coefficient may introduce minor apparent cohesion and reduced permeability compared to clean sands with low fines.

Prior to model preparation, laboratory tests on the sand (e.g., direct shear) were consulted to determine its peak friction angle at various densities. For simulation of in-situ sandy seabed layer, a target relative density (D_r) of about 36.4% and 73.2% were selected for silica sand (No. 7) with peak internal friction angles ranging from 38.6° to 43.6°. A silica sand with silt (No. 8) was characterized by peak internal friction angle of 34.1° at a relative density of 34.8%, aligning with silty conditions of the offshore site. Table 5 summarizes geotechnical properties of both silica sands used in this study.

Table 5. Index properties of silica sand (No. 7) and silica sand with silt (No. 8)

An automatic pluviation apparatus was employed to establish consistent sand deposits within the strongbox per SPS-F KOCED guidelines. As can be seen in Figure 7, key pluviation parameters such as diffuser tank speed, nozzle diameter, and drop height were calibrated through trial tests with real-time laser sensor height adjustments ensuring precise control of deposit thickness. Several trials confirmed the repeatability of the target densities and minimal

layering effects. Several guide angles were installed on the edges of the strongbox to minimize the boundary effects from sliding sands.

Figure 7. Assessment of pluviation parameters for consistent ground densities across centrifuge tests

Upon achieving the desired soil profile, a miniature cone penetration test (mCPT) was conducted in-flight at 70 g to characterize the sand's in situ density and strength prior to vibration test commencement. A 10 mm diameter miniature cone penetrated to a depth of 100 mm at a rate of 1.2 mm/s (model scale), compliant with SPS-F KOCED guidelines. By comparing the measured cone tip resistances with empirical correlations, the shear-wave velocity of the model ground was inferred, providing in-flight verification of soil characteristics:

$$V_s = Y(q_c)^j, \tag{22}$$

where q_c cone tip resistance (MPa), Y empirical constant (dimensionless), j exponent (dimensionless). The parameter Y is known to be affected by grain characteristics, soil compressibility, age, and cementation. In this study, best-fit power correlation by the regression for the exponent of 0.23 was used. The small-strain shear modulus was calculated by:

$$G_0 = \rho \cdot V_s^2, \tag{23}$$

where G_0 small-strain shear modulus (MPa), ρ soil density (kg/m³), V_s shear wave velocity (m/s) obtained by empirical correlations (Kim et al., 2017).

Although the prototype field site comprises of three-layer stratigraphy, one homogeneous sand layer was used in the centrifuge, representing a simplified version for experimental reproducibility. This homogenization accounts for observed differences in shallow q_c and G_0 versus field CPTs (Figure 8), attributable to unmodeled clay effects, yet achieves close agreement at the reference depth of z = 5 m to benchmark G_0 in subsequent analyses.

The calculated small-strain shear modulus values from cone penetration measurements in centrifuge experiments were compared with those obtained from field sites (SB-1, SB-2, SB-3). As shown in Figure 8, centrifuge q_c and G_0 profiles diverge from field data near the surface due to absent clay-induced softening but converge at the reference depth z = -5 m despite moderate differences, validating the centrifuge model's utility as a reference for stiffness calculations in homogeneous conditions.

Figure 8. Comparison of cone resistance profiles and estimated shear modulus from centrifuge and field tests at the prototype site at reference depth z = -5 m

Local scour was modeled by sequentially removing sand from around each of the three suction buckets between centrifuge test runs (as described in Section 3.1), with geometry replicated from field-observed patterns via multi-beam sonar bathymetry data obtained from KEPCO. Conical scour holes were excavated concentrically aroundd the bucket's perimeter, with radius r and angle of repose φ estimated per Stuyts et al. (2013):

$$r = \frac{D}{2} + \frac{S}{\tan \varphi}\,, \tag{24}$$

where S is scour depth and φ (≈ half of the sands' internal friction angles per Achmus et al., 2010). Maximum targeted S fell within a reasonable range of 0.4–0.6 D (bucket diameter D), based on field observations.

Post excavation, precision depth gauges were employed to ensure that the scour excavation adhered rigorously to predefined target depths across all three buckets. An average value of scour depth was reported. Progressive stages—Scour Stages 1–4 (targeted $S/D \approx 0$, 0.2–0.3, 0.3–0.5, 0.5–0.6; measured means 0, 0.20–0.30, 0.33–0.49, 0.49–0.61—enabled systematic assessment. These modifications were performed carefully on the centrifuge flight room without re-installation of buckets. This structured approach ensured a systematic investigation of the effects of progressive scour on the dynamic response of the suction buckets under controlled centrifuge conditions. Figure 9 compares these model scour profiles (conical holes, radially profiled near each bucket) with prototype depths from multi-beam surveys (depths as below-seabed distances, referenced to estimated seabed level). Here, vertical dashed lines denote bucket edges at $\pm D/2$, and gray lines indicate depths below estimated seabed level around the bucket foundation. Similarly, in centrifuge modelling, scour depth profile was obtained using a 2D laser sensor profiler which measures distance from the referenced level.

Figure 9. Comparison of scour profiles. (a) Seabed depth profiles from field multi-beam survey, taken radially near the bucket; vertical dashed lines represent the bucket edges; (b) scour profile in centrifuge measured by a laser sensor.

3.4 Dynamic load modelling

The dynamic loading on the model was applied using an amplified piezoelectric actuator APA440MML (Cedrat Technologies, 2015), chosen based on the recommendations of Cabrera et al. (2012). The assembly was designed following Futai et al. (2018) and Kariyawasam (2020). A function generator (controlled through a MATLAB-based script) was used to send different types of voltage waveforms to the actuator's driver amplifier LA75C to produce free vibration, sine, and square waves in different frequency (Figure 10). The frequency range was chosen based on initial estimates of the natural frequency – for example, between 1 Hz and 5 Hz in model scale (which corresponds to about 0.014–0.071 Hz in prototype scale).

Figure 10. Illustration of the voltage waveforms applied in-flight using piezoelecric actuator

Prior to testing, the piezoelectric actuator was calibrated to establish the relationship between input voltage and force output. Load magnitudes were controlled via different voltage signal types (See Fig. 10) to replicate realistic wind-induced loading, informed by integrated load analysis (ILA) results from BLADED software for Serviceability

Limit State (SLS) and Ultimate Limit State (ULS) conditions. The ILA used prototype model parameters (U-136 4.2 MW OWT) for Design Load Cases (DLCs) per IEC 61400-3; details are not reported here due to nondisclosure agreement with KEPCO.

Figure 11 shows time histories of the applied dynamic load from the piezoelectric actuator and the resulting bending moment at the tower base, calculated from strain gauge measurements at the tower cross-section. Bending moment values were compared from ILA results (from BLADED) at the foundation reference point to match the strain gauge location. The square-type signal ensured experimental responses mimic OWT behavior under sudden loads (e.g., wind gusts) during non-operating or stormy conditions, with peak moments within ULS limits, and the sine wave signals produced consistent response mimicing normal operating conditions within SLS limits.

Figure 11. Time histories from dynamic loading. (a) Dynamic load input from piezoelectric actuator; (b) Corresponding bending moment response from strain measurement at tower base

4. Analytical frameworks for scour sensitivity

4.1 Scour sensitivity of natural frequency

Sensitivity analysis provides a systematic way to quantify how changes in input parameters influence a system's output. In this study, we emphasize how changes in scour depth around a foundation affect the dynamic properties of a structure, specifically its natural frequency.

Consider a system where the output $f \in \mathbb{R}^{n}$ depends on multiple input parameters $\mathrm{x}_1, x_2, \ldots x_n$, expressed as $f = f(\mathrm{x})$. In the context of offshore wind turbines, f could represent the natural frequency, and the inputs might include scour depth, structural mass, or foundation stiffness. The scour sensitivity of natural frequency S_f is defined by the partial derivative:

$$S_f = \left.\frac{\partial f}{\partial \mathrm{S}}\right|_{S=S_0} \tag{1}$$

where f is natural frequency (Hz), S is scour depth (m), and the subscript indicates evaluation at nominal values. This partial derivative indicates how f changes in response to a small perturbation in S, assuming all other parameters remain constant. To compare the relative importance across parameters with different units or scales, the relative (or normalized) sensitivity S_{rel} can be employed:

$$S_{rel} = \left|\frac{\partial f}{\partial S} \cdot \frac{S}{f}\right|_{S=S_0} \tag{2}$$

Such relative measure facilitates the ranking of other important parameters by impact on the output.

4.2. Linear approximation for scour sensitivity

To evaluate scour-induced natural frequency shifts in OWTs supported by tripod bucket suction foundations, a simplified structural model based on the single-degree-of-freedom (SDOF) cantilever beam analogy by Van der Tempel & Molenaar (2002) is adopted for fixed-base natural frequency estimation:

$$f = \frac{1}{2\pi}\sqrt{\frac{3.04EI}{L^3(M_{RNA} + 0.227M_t)}} \tag{3}$$

where EI denotes flexural rigidity (Nm²), L is length of tower (m), M_{RNA} is the rotor-nacelle assembly mass (kg), and M_t is the mass of the tower (kg). Assuming scour increases effective length L of the structure (i.e., $L = L_0 + S$), the scour sensitivity of natural frequency f with respect to scour depth S is analytically expressed as:

$$\frac{\partial f}{\partial S} = -\frac{3}{4\pi}\sqrt{\left(\frac{3.04EI}{M_{RNA} + 0.227M_t}\right)}(L_0 + S)^{-\frac{5}{2}} \tag{4}$$

Since $f \propto L^{-3/2}$, the relative natural frequency change due to scour is approximated as:

$$\frac{\Delta f}{f_0} = \left(1 + \frac{S}{L_0}\right)^{-\frac{3}{2}} - 1 \tag{5}$$

For small scour-to-length ratio $S/L_0 \ll 1$, a Taylor expansion of $\left(1 + \frac{S}{L_0}\right)^{-3/2}$ about zero provides:

$$\frac{\Delta f}{f_0} \approx \left(1 - \frac{3}{2}\frac{S}{L_0} + \frac{15}{8}\left(\frac{S}{L_0}\right)^2 - \cdots\right) - 1 \tag{6}$$

Truncating higher-order terms leads to a simple linear relationship. Defining a dimensionless scour depth ratio S/D, where D is the foundation diameter, the relative natural frequency shifts can be approximated by:

$$\frac{\Delta f}{f_0} = \frac{f - f_0}{f_0} = a \cdot \frac{S}{D} \tag{7}$$

where a is a constant representing the scour sensitivity of natural frequency. By inspection of the first-order term in Taylor expansion, one obtains:

$$a \approx -\frac{3}{2}\frac{D}{L_0} \tag{8}$$

This linear model implies that a 1% increase in tower length L_0 due to scour causes a 1.5×D% decrease in the natural frequency, underscoring the pronounced effect of scour on modal properties. Here, length units are in meters. While a can serve as a proxy for scour-induced changes in the natural frequency, foundation-specific complexities may necessitate more refined models.

4.3 Scour sensitivity incorporating soil structure interaction

Although the linear model offers a straightforward way to estimate how scour shifts the natural frequency, the assumption of a rigid foundation base can be overly simplistic. Real scour conditions may vary locally, and multi-footing structures could be exposed to asymmetrical scour conditions.

In reality, soil–structure interaction (SSI) becomes significant, particularly with the reduction of foundation embedment and thus its stiffness properties. To address these effects, an extended formulation is employed to incorporate foundation flexibility in scour sensitivity analysis.

Using Dunkerley's method, the natural frequency of an OWT with a flexible foundation can be written as:

$$\frac{1}{f_{SSI}^2} = \frac{1}{f_{FB}^2} + \frac{1}{f_\theta^2} \tag{9}$$

where f_{FB} is fixed-base natural frequency (i.e., the cantilever mode with tip mass), and $f_\theta = \frac{1}{2\pi}\sqrt{\frac{k_\theta}{I_\theta}}$ represents the rocking frequency associated with the TSB foundation's rocking stiffness k_θ (Nm/rad) and the moment of inertia about the rocking axis I_θ (kgm^2).

Applying chain rule with foundation's rocking stiffness k_θ, the scour sensitivity of natural frequency considering SSI can be computed:

$$\frac{\partial f_{SSI}}{\partial S} = \frac{\partial f_{SSI}}{\partial k_\theta} \times \frac{\partial k_\theta}{\partial S} \tag{10}$$

Assuming $f_{SSI} = f_{FB} \cdot (1+\kappa)^{-1/2}$ (after Veletsos & Meek, 1974), the first term can be found by

$$\frac{\partial f_{SSI}}{\partial k_\theta} = \frac{\beta^2}{2}\frac{f_{SSI}}{k_\theta}\kappa \tag{11}$$

where $\kappa = k_s/k_\theta$ denotes the structure-foundation stiffness ratio, and $\beta = f_{SSI}/f_{FB}$ is defined as the ratio of flexible-base natural frequency to that of fixed-base (Futai et al., 2018). Hence, scour sensitivity of natural frequency including soil-structural interaction is given by:

$$\frac{\partial f_{SSI}}{\partial S} = -\frac{(1-\beta^2)}{2}\frac{f_{SSI}}{k_\theta}\frac{\partial k_\theta}{\partial S} \tag{12}$$

For a rigid circular foundation embedded in an elastic half-space, rocking stiffness k_θ is controlled by soil moment-rotation compatibility and often scales with the cube of the foundation diameter (Gazetas, 1983; DNV, 2021; Bell 1991):

$$k_\theta \propto G_0 D^3 \tag{13}$$

where k_θ is the foundation rocking stiffness, G_0 is the shear modulus of soil, and ν_s is the soil Poisson's ratio.

However, if the influence of scour on foundation stiffness is non-trivial, the relationship between k_θ and S may deviate from linearity. To allow soil non-linearity, stress redistribution, and bucket skirt edge fixity in TSB foundations, the rocking stiffness is assumed to vary nonlinearly with scour:

$$k_\theta(S) = k_{0,\theta} \cdot \left[1 - \left(\frac{S}{D}\right)^q\right], \qquad k_{0,\theta} = \frac{1}{2} N_c R^2 k_v \tag{14}$$

where q is an embedment exponent (dimensionless), N_c considers the tripod's group effects as discussed in Kim et al. (2014); and R is the radial distance (m) from the center to each tripod leg. For the values of $k_{0,\theta}$, this study employed discrete vertical springs whose stiffness was given by Poulos & Davis (1974):

$$k_v = 2G_0 D/(1 - \nu_s)$$

where k_v is vertical spring stiffness (N/m), G_0 is the shear modulus of soil (MPa), calculated following guidelines in OWA (2019) using stiffness factors of 200–600 and an exponent of 0.5 for sand, and Poisson's ratio of soil $\nu_s = 0.25$.

Here, $k_\theta(S)$ denotes the rocking stiffness of the foundation as a function of scour depth; $k_{0,\theta}$ is its initial value prior to any scour (i.e., at S = 0). The scour depth ratio S/D normalizes the scour depth S (as the vertical distance of soil removal below the original seabed level) by the bucket diameter D, allowing comparison across foundation scales. These parameters capture how progressive scour reduces rocking stiffness of foundation k_θ nonlinearly. It is noted that as scour progresses, relative dominance of structure's stiffness over foundation stiffness grows nonlinearly. To illustrate this, normalized rocking stiffness as a function of scour depth ratio is depicted in Figure 12, resulting in greater flexibility and SSI effects and critically impacting scour sensitivity with dynamic performance.

Figure 12. Normalized rocking stiffness k_θ/GD (where k_θ is the current rocking stiffness) as a function of normalized scour depth S/D. The curve illustrates a nonlinear reduction of foundation stiffness due to progressive scour

The scour sensitivity of the rotational stiffness of foundation then becomes:

$$\frac{\partial k_\theta}{\partial S} = -\frac{q k_{0,\theta}}{D} \cdot \left(\frac{S}{D}\right)^{q-1} \tag{15}$$

The partial derivative of the natural frequency considering SSI with respect to scour is as follows:

$$\frac{\partial f_{SSI}}{\partial S} = -\frac{(1-\beta^2)q}{2D} \cdot \frac{f_{SSI}(S/D)^{q-1}}{1-(S/D)^q} \tag{16}$$

Evaluating at the initial state (i.e. $S = 0$), the relative natural frequency change is :

$$\frac{\Delta f}{f_0} = \frac{f_{SSI} - f_{0,SSI}}{f_{0,SSI}} = \left[1 - \left(\frac{S}{D}\right)^q\right]^p - 1, \qquad p = \frac{(1-\beta_0^2)}{2} \tag{17}$$

where $f_{0,SSI}$ denotes the initial natural frequency considering SSI, and β_0 is the initial foundation flexibility (1/stiffness). This expression quantifies how the natural frequency shifts as scour depth increases relative to the reference state.

To further explore this relationship, expanding the bracket in a binomial (or Maclaurin) series in Eqn. (17) yields:

$$\frac{\Delta f}{f_0} = -p(S/D)^q + \frac{p(p-1)}{2}(S/D)^{2q} + \cdots + \mathcal{O} \tag{18}$$

By truncating higher-order terms and retaining the leading term, we derive a simplified approximation:

$$\frac{\Delta f}{f_0} \approx -p(S/D)^q \tag{19}$$

This approximation holds reasonably well for $S/D \ll 1$; however, its accuracy diminishes as scour depth increases due to the neglected nonlinear contributions. To address this limitation, we propose a two-parameter power law model:

$$\frac{\Delta f}{f_0} \approx a\left(\frac{S}{D}\right)^b, \tag{20}$$

where $a < 0$ is a constant encapsulating the scour sensitivity inherently tied to SSI effects through the parameter p, while $b \geq 1$ reflects the nonlinearity influenced by the embedment exponent q. The parameters a and b can be determined empirically (e.g., by centrifuge tests or field data).

In summary, this approach enhances the understanding of scour-induced natural frequency shifts, providing a robust framework for predicting structural responses in geotechnical engineering applications. Although a simple predictive model offers insight into how scour depth affects OWT natural frequency, capturing the role of soil–structure interaction demands more sophisticated stiffness models. Depending on the magnitude of scour and the foundation type, other relationships may better describe the scour-induced degradation in rocking foundation stiffness of TSB foundations.

5. **Results**

5.1 Determination of natural frequency

Natural frequencies were derived from acceleration data recorded by MEMS accelerometers (ADXL1003 series) positioned along the tower, as described in Section 3.1. Power spectral density (PSD) analysis, employing Welch's method with segmented time series, was used to identify the natural frequencies. Due to the large volume of data and the need to distinguish meaningful response from background noise, a structured data processing pipeline was implemented. In particular, ambient and forced-vibrations measured by accelerometers for whole testing time were

divided into segments with identification of different input voltage signal waveforms, and each segment's periodogram was computed using Welch's method. In order to facilitate the identification of natural frequencies, summation of the PSDs from several accelerometers was used for improved the signal-to-noise ratio and enhanced the prominence of structural modes. Moreover, the frequency-domain analyses were carefully checked for any spectral leakage to ensure sharp frequency resolution. Across all centrifuge tests, clear modal peaks allowed accurate identification of natural frequencies for the analysis of scour sensitivity. Table 6 summarizes experimentally measured natural frequencies at four different scour depth ratios (S/D = 0 to 0.6), spanning across three different soil conditions (G_0 = 61.49, 32.37, 38.83 MPa).

Table 6. Centrifuge experiment results: f_1 first natural frequency (Hz), f_2 second natural frequency (Hz), G_0 initial shear modulus (MPa), S/D scour depth ratio

5.2 Effect of scour on natural frequency

Figure 13. Variation of the natural frequencies (Mode 1 and Mode 2) with increasing scour depth ratio (S/D)

Figure 13 illustrates the reduction in measured natural frequencies with scour depth ratios. In T1, the natural frequency (Mode 1) decreased from 0.160 Hz to 0.152 Hz, a 5.0% reduction, while Mode 2 dropped by 3.8% (from 1.535 Hz to 1.477 Hz). Similarly, measurements from T2 and T3 exhibited comparable reductions of 5.3% (0.152 Hz to 0.144 Hz) and 5.2% (0.154 Hz to 0.146 Hz), for respective modes, while Mode 2 dropped by 3.8% (from 1.469 to 1.413 Hz) and 5.3% (from 1.510 Hz to 1.430 Hz). For all test series, progressive increases in scour depth ratios led to a consistent downward shift in both natural frequencies, confirming scour-induced stiffness loss as outlined in Section 5.3. Notably, the second mode natural frequency exhibited a relatively nonlinear drop compared to the first mode, suggesting higher sensitivity and volatility to scour, likely due to dependence on higher-order structural dynamics with localized effects on foundation. The variability of natural frequencies between the three tests (T1–T3) also underlines the dependence on the initial soil stiffness, highlighting the importance of considering soil-structure interaction across varying soil conditions.

By comparing experimental relative natural frequency shifts ($\Delta f/f_0$) with a power-law model $\Delta f/f_0 = a(S/D)^{\mathrm{b}}$, where a and b power-law parameters (dimensionless), as outlined in Section 5.3, validated aforementioned findings with fitted parameters (e.g., T1: a = -0.110, b = 1.106; T2: a = -0.133, b = 1.944). The experimental results showed that the value of $\Delta f/f_0$ reached -0.05 at S/D=0.48 for T1, closely matching the prediction. The nonlinear power-law model outperformed the linear approximation $a(S/D)$, capturing neglected SSI effects by fixed-base models (Section 5.2). Specifically, the exponent b exhibited elevated values for T2 and T3 relative to T1, indicating variations associated with initial foundation stiffness. However, clear deviations between theoretical and experimental data at higher scour depths illustrate complex interactions between scour progression, foundation flexibility, and natural frequency responses for OWT with TSB foundations. Thus, accurate incorporation of nonlinear effects with SSI

becomes more critical in providing reliable assessments for scour-induced natural frequency changes in offshore wind turbines supported by various foundation types.

Figure 14. Relative natural frequency change as a function of S/D, compared with a power-law model

5.3 Comparison with field measurements

Complementing the centrifuge data, field measurements from existing studies were integrated for validation of results, each represented by distinct symbols to differentiate origins and methodologies. In Figure 15, comparative analysis with published data showcased TSB's reductions (5–6%) versus monopiles (5–10% at S/D =1), suggesting different scour risks posed due to load redistribution among its multi-footing design. Field data from Taiwan Mast (Tseng et al., 2018) and Belwind (Weijtjens et al., 2017) provided empirical observations of natural frequencies for scour depth ratios up to 2.0, derived from operational wind farms and Taiwan Mast, with the reported values normalized using the same methodology laid out in this study to ensure comparability. For a cohesive and reliable comparison of scour impacts on natural frequency, the normalized values of S/D were used, avoiding the influence of different foundation types and sizes. These diverse sources collectively highlight the variability in scour response across different contexts, mitigating discrepancies arising from differing turbine designs and operational complexities in field studies. The comprehensive synthesis situates this study's alignment within broader scope in scour-based monitoring research for OWTs and real-world relevance, while centrifuge test data provides a controlled benchmark for predictive insights.

Figure 15. Comparison of relative natural frequency shifts ($\Delta f/f_0$, where f_0 is initial frequency) with normalized scour depth *S*/*D* between this study's centrifuge tests (TSB foundation) and reported field data (monopile and met mast)

6. Discussion

6.1 Measured scour sensitivities

Utilizing the centrifuge test measurements, scour sensitivities ($\partial f/\partial S$) were analyzed. Scour sensitivity coefficients, defined via partial derivatives in Section 4.1, were calculated by differential values of the natural frequencies and scour depths. The result showed an increasingly negative trend with increasing scour levels across all centrifuge test series. As can be seen in Figure 16, T1's higher initial stiffness resulted in a less steep sensitivity curve, indicating that more flexible foundation stiffness amplifies the relative influence of scour on structural dynamics.

Figure 16. Scour sensitivity coefficients ($\partial f/\partial S$) across different soil conditions and foundation flexibility β as a function of scour depth ratio (S/D)

Figure 16 further elucidates this by linking increased foundation flexibility β with increased scour sensitivity, highlighting a nonlinear interplay critical for TSB foundations. As scour depth ratios S/D increased, the foundation flexibility β showed a consistent decrease with increasing scour levels, while scour sensitivity grew more negative, reflecting heightened natural frequency responsiveness. In contrast to T1, test cases T2 and T3 showed the steeper shifts, revealing higher nonlinearity by SSI effects in TSB foundations.

The integration of flexibility and sensitivity metrics advances the understanding of scour's impact on higher order structural dynamics for TSB foundations, offering a differing perspective beyond monopile-based studies. Such insights stress the importance of initial soil stiffness and different structural configurations on scour sensitivity. As a measure supporting frequency-based structural health monitoring, scour sensitivity quantified scour's dynamic impact on natural frequencies and elucidated foundation-specific vulnerabilities, unique to TSB foundations for advanced scour monitoring strategies with calibrated data. Analyzing distinct trends considering SSI with various soil conditions would enhance the understanding of multi-footing structure's scour impacts.

6.2 Calibration of the proposed model

The scour-induced natural frequency shift was correlated to the non-dimensional scour depth ratio through the power-law expression introduced in Eq. (18). Non-linear least-squares fitting of the centrifuge data for the tripod bucket suction foundation produced:

$$a \approx -0.12, \qquad b \approx 1.5 \tag{21}$$

where a and b are power-law parameters (dimensionless). The exponent $b \approx 1.5$ is consistent with the embedment-dependent rocking stiffness formulation when the embedment exponent is $q = 3$ (i.e. $b = q/2$), as reported in recent centrifuge and finite-element studies of tripod suction bucket foundations (Jeong et al., 2021; Kim et al., 2023). The negative coefficient affirms the monotonic reduction of the first natural frequency with increasing scour depth, while the magnitude of b reflects the pronounced nonlinearity introduced by reduction in rotational stiffness.

Calibration using field measurements in relevant literature for monopile-supported offshore wind turbines yielded:

$$a \approx -0.06, \qquad b \approx 1.0 \tag{22}$$

The unity exponent b indicates an approximately linear relationship between scour depth and natural frequency reduction, implying that monopile systems experience less pronounced non-linear stiffness degradation than TSB foundations. Furthermore, the magnitude a is roughly one-half of that obtained for the tripod suction bucket system, suggesting that for identical S/D, monopile exhibit about 50% of the relative natural frequency loss observed in TSB

foundations. The calibration process is illustrated in Figure 17, which depicts the fitted power-law curves alongside experimental data from centrifuge tests for TSB foundations and field measurements for monopile foundations.

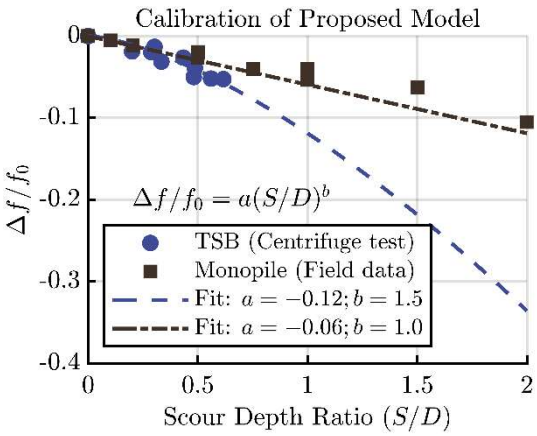

Figure 17. Calibration using centrifuge results for TSB foundations and field data for monopile foundations

However, direct comparison between the two foundation types must be interpreted with caution because the normalization in S/D may have used different diameter scales. Given the disparity between tripod suction buckets and monopiles, an "effective diameter" that reflects more robust scaling would provide a more rigorous basis for cross-type comparison. Development and validation of such a normalization scheme lie beyond the scope of the present study and are identified as a topic for future research.

6.3 Second Mode Sensitivity to Scour in Tripod Suction Bucket Foundations

To expand on these findings, the second natural frequency (Mode 2) was analyzed similarly to the first (Mode 1), using the same sensitivity framework (Section 4.1) and power-law fitting (Eq. 18). For Mode 2, centrifuge data showed reductions up to 3.8–5.3% across tests T1–T3 at *S*/*D* up to 0.6, but with a more inconsistent relative decrease compared to Mode 1 (e.g., less linear reductions). This heightened volatility arises because Mode 2, involving more complex bending and torsional components, is particularly vulnerable to local stiffness asymmetries introduced by scour in multi-footing systems like the TSB foundations. Unlike Mode 1's global response, which benefits from stress redistribution among the three buckets, Mode 2 amplifies uneven soil support loss (e.g., deeper scour at one leg), leading to modal splitting and greater uncertainties in the frequency shifts. These results tie directly into structural health monitoring, emphasizing the need to track both Mode 1 and Mode 2 for early scour detection for the warning of the localized scour risks, which could otherwise lead to resonance with rotor excitations and reduced OWT lifespan.

7. Conclusion

In this study, we elucidated the scour sensitivity of a 4.2 MW offshore wind turbine supported by a tripod suction bucket foundation in sandy soil through geotechnical centrifuge experiments at 70 g, addressing a critical gap in understanding multi-footing structural dynamics. This paper introduces a scour sensitivity parameter that quantifies the rate of natural frequency change with scour, offering a practical metric for frequency-based structural health monitoring. In conclusion, the main findings of this study can be summarized as follows:

1) The centrifuge model experiments were conducted with accurate replication of the prototype conditions (i.e., structural properties, various soil conditions, realistic scour shapes and dynamic loading). This rigorous modelling approach yielded dependable results, aligning well with field conditions despite moderate discrepancies.
2) The results from centrifuge tests systematically quantified the reduction in natural frequencies with increasing scour depth (S/D up to 0.6), revealing a maximum 5.3% drop in first natural frequency and a more pronounced volatility in second natural frequency due to its higher sensitivity to local asymmetries and stiffness changes in multi-footing systems.
3) These findings underscore the importance of monitoring both first and second natural frequencies for early detection of scour-induced asymmetries in multi-footing OWT foundations, ultimately enhancing structural health monitoring strategies, maintenance practices, and the operational lifespan of offshore wind infrastructure.
4) A scour sensitivity parameter was formulated, expressed as a power-law relationship between the relative change in natural frequency and the scour depth ratio, enabling quantitative assessment of scour impacts on the natural frequency incorporating SSI effects. The power-law model incorporating soil-structural interaction entails two parameters for capturing nonlinear trends in natural frequency shifts.
5) Comparative analyses of the proposed scour sensitivity formula against centrifuge test data affirmed high accuracy and reliability, particularly in accounting for the complex interactions between soil, structure, and scour in offshore foundations.

Funding

This research was supported by Korea Electric power Corporation. (Grant number: R23XO05-01). This research was supported by the Mid-Career Researcher Program funded by the National Research Foundations of Korea (NRF-2022R1A2C2009260). This research was supported by Korea Institute of Marine Science & Technology Promotion (KIMST) funded by the Ministry of Oceans and Fisheries, Korea (RS-2025-02304428). This research was supported by the BK21 FOUR (Fostering Outstanding Universities for Research) funded by the Ministry of Education(MOE, Korea) and National Research Foundation of Korea (NRF). In addition, this work was supported by the Korea Institute of Energy Technology Evaluation and Planning (KETEP) and the Ministry of Trade, Industry & Energy (MOTIE) of the Republic of Korea (NO. RS-2025-02318006).

References

Achmus, M., Kuo, Y. S., & Abdel-Rahman, K. (2010). Numerical investigation of scour effect on lateral resistance of windfarm monopiles. In *ISOPE International Ocean and Polar Engineering Conference, Beijing, China.*

Arany, L., Bhattacharya, S., Macdonald, J. H., & Hogan, S. J. (2016). Closed form solution of Eigen frequency of monopile supported offshore wind turbines in deeper waters incorporating stiffness of substructure and SSI. *Soil Dynamics and Earthquake Engineering*, *83*, 18-32.

Bell, R., & Bell, R. W. (1991). The analysis of offshore foundations subjected to combined loading (Doctoral dissertation, University of Oxford).

Bel-Hadj, Y., Weil, M., Weijtjens, W., & Devriendt, C. (2024). Experimental validation of automated OMA and mode tracking for structural health monitoring of transmission towers. *Structural Health Monitoring*. https://doi.org/10.1177/14759217241249048.

Bhattacharya, S. (2019). Design of foundations for offshore wind turbines. John Wiley & Sons.

Cabrera, M. A., Caicedo, B., & Thorel, L. (2012). Dynamic actuator for centrifuge modeling of soil-structure interaction. *Geotechnical Testing Journal*, *35*(4), 539-547.

Cedrat Technologies (2015). APA440MML amplified piezoelectric actuator technical manual. Cedrat Technologies.

DNV. (2021). Offshore Soil Mechanics and Geotechnical Engineering (Recommended Practice DNV-RP-C212).

Futai, M. M., Dong, J., Haigh, S. K., & Madabhushi, S. P. G. (2018). Dynamic response of monopiles in sand using centrifuge modelling. Soil Dynamics and Earthquake Engineering, 115, 90-103.

Futai, M. M., Haigh, S. K., & Madabhushi, G. S. (2021). Comparison of the dynamic responses of monopiles and gravity base foundations for offshore wind turbines in sand using centrifuge modelling. *Soils and Foundations*, *61*(1), 50-63.

Gazetas, G. (1983). Analysis of machine foundation vibrations: state of the art. International Journal of soil dynamics and earthquake engineering, 2(1), 2-42.

Houlsby, G. T. (2016). Interactions in offshore foundation design. *Geotechnique*, *66*(10), 791-825.

Jalbi, S., & Bhattacharya, S. (2018). Closed form solution for the first natural frequency of offshore wind turbine jackets supported on multiple foundations incorporating soil-structure interaction. *Soil Dynamics and Earthquake Engineering*, *113*, 593-613.

Jalbi, S., Nikitas, G., Bhattacharya, S., & Alexander, N. (2019). Dynamic design considerations for offshore wind turbine jackets supported on multiple foundations. *Marine structures*, *67*, 102631.

Jawalageri, S., Prendergast, L. J., Jalilvand, S., & Malekjafarian, A. (2022). Effect of scour erosion on mode shapes of a 5 MW monopile-supported offshore wind turbine. *Ocean Engineering*, *266*, 113131.

Jeong, Y. H., Kim, J. H., Park, H. J., & Kim, D. S. (2019). Cyclic behavior of unit bucket for tripod foundation system supporting offshore wind turbine via model tests. Wind Energy, 22(2), 257-268.

Jeong, Y. H., Ko, K. W., Kim, D. S., & Kim, J. H. (2021). Studies on cyclic behavior of tripod suction bucket foundation system supporting offshore wind turbine using centrifuge model test. *Wind Energy*, *24*(5), 515-529.

Kallehave, D., Byrne, B. W., LeBlanc Thilsted, C., & Mikkelsen, K. K. (2015). Optimization of monopiles for offshore wind turbines. Philosophical Transactions of the Royal Society A: Mathematical, Physical and Engineering Sciences, 373(2035), 20140100.

Kariyawasam, K. D., Middleton, C. R., Madabhushi, G., Haigh, S. K., & Talbot, J. P. (2020). Assessment of bridge natural frequency as an indicator of scour using centrifuge modelling. *Journal of Civil Structural Health Monitoring*, *10*, 861-881.

KEPRI (2015). Geological survey report on candidate site for suction bucket offshore wind turbine. *Korea Electric Power Research Institute. (KEPRI): Daejeon, Korea.*

KEPRI (2016). Test bed for 2.5 GW offshore wind farm at yellow sea design basis. *Final Report. Korea Electric Power Research Institute. (KEPRI): Daejeon, Korea*.

KEPRI (2020). Structural calculation report for offshore wind turbine MMB support foundation. *Final Report. Korea Electric Power Research Institute. (KEPRI): Daejeon, Korea*.

KOWP (2021). Geological survey report on the feasibility study of the southwestrn sea offshore wind farm. *Korea Offshore Wind Power.*

Kim, D. J., Choo, Y. W., Kim, J. H., Kim, S., & Kim, D. S. (2014). Investigation of monotonic and cyclic behavior of tripod suction bucket foundations for offshore wind towers using centrifuge modeling. *Journal of Geotechnical and Geoenvironmental Engineering*, *140*(5), 04014008.

Kim, D. S., Kim, N. R., Choo, Y. W., & Cho, G. C. (2013). A newly developed state-of-the-art geotechnical centrifuge in Korea. *KSCE journal of Civil Engineering*, *17*(1), 77-84.

Kim, J. H., Choo, Y. W., & Kim, D. S. (2017). Correlation between the shear-wave velocity and tip resistance of quartz sand in a centrifuge. *Journal of Geotechnical and Geoenvironmental Engineering*, *143*(11), 04017083.

Kim, K. S., Hwang, B. Y., Lee, M. H., & Kim, S. R. (2023). Effect of Scour Depth on Natural Frequency of Offshore Wind Turbine with Tripod Suction Bucket Foundation. In International Conference on Geotechnics for Sustainable Infrastructure Development (pp. 2745-2758). Singapore: Springer Nature Singapore.

Kim, S. R., & Oh, M. (2014). Group effect on bearing capacities of tripod bucket foundations in undrained clay. *Ocean engineering*, *79*, 1-9.

Kutter, B. L. (1992). Dynamic centrifuge modeling of geotechnical structures. *Transportation research record*, (1336).

Li, Q., Prendergast, L. J., Gavin, K. G., Askarinejad, A., & Wang, X. Q. (2024). A method to quantify the beneficial effect of scour protection on lateral behaviour of monopiles for offshore wind turbines. *Ocean Engineering*, *307*, 118196.

Liang, F., Zheng, H., & Zhang, H. (2020). On the pile tension capacity of scoured tripod foundation supporting offshore wind turbines. *Applied Ocean Research*, *102*, 102323.

Ma, H., Yang, J., & Chen, L. (2018). Effect of scour on the structural response of an offshore wind turbine supported on tripod foundation. *Applied Ocean Research*, *73*, 179-189.

OWA. (2019). Suction installed caisson foundations for offshore wind: design guidelines. Offshore Wind Accelerator.

Poulos, H. G., & Davis, E. H. (1974). Elastic solutions for soil and rock mechanics. John Wiley & Sons.

Qi, W. G., & Gao, F. P. (2019). Local scour around a monopile foundation for offshore wind turbines and scour effects on structural responses. In *Geotechnical engineering-advances in soil mechanics and foundation engineering*. IntechOpen.

Qi, W. G., Gao, F. P., Randolph, M. F., & Lehane, B. M. (2016). Scour effects on p–y curves for shallowly embedded piles in sand. *Géotechnique*, *66*(8), 648-660.

Robertson, P. K. (2009). Interpretation of cone penetration tests—a unified approach. *Canadian geotechnical journal*, *46*(11), 1337-1355.

Ryu, M. S., Lee, J. S., Kwag, D. J., & Seo, Y. H. (2019). Verification of tripod suction pile applicability through dynamic characteristic analysis of offshore wind turbine at each installation stage. *Journal of wind energy*, *10*(3), 12-21. https://doi.org/10.33519/kwea.2019.10.3.002

Ryu, M. S., Jung, M. U., Lee, J. S., & Kim, D. S. (2020). Closed form solutions for predicting lateral response of tripod suction pile for offshore wind turbine foundation. *Energies*, *13*(23), 6176.

Ryu, M. S., Kim, S. R., Cho, D. H., & Kang, J. G. (2022). Innovative single-day installation vessel for offshore wind turbines. *Energies*, *15*(11), 3914. https://doi.org/10.3390/en15113914

Seo, Y. H., Ryu, M. S., & Oh, K. Y. (2020). Dynamic Characteristics of an Offshore Wind Turbine with Tripod Suction Buckets via Full-Scale Testing. *Complexity*, *2020*(1). https://doi.org/10.1155/2020/3079308

Stroescu, I. E., Frigaard, P., & Fejerskov, M. (2016). Scour development around bucket foundations. *International journal of offshore and polar engineering*, *26*(01), 57-64.

Stuyts, B., Cathie, D., & Xie, Y. (2013). Scour assessment and measurements for pile-supported wind turbine foundations. In *International Conference on Offshore Mechanics and Arctic Engineering* (Vol. 55409, p. V006T10A025). American Society of Mechanical Engineers.

Stuyts, B., & Suryasentana, S. (2023). Applications of data science in offshore geotechnical engineering: State of practice and future perspectives. In *SUT Offshore Site Investigation and Geotechnics*.

Skau, K. S., Grimstad, G., Page, A. M., Eiksund, G. R., & Jostad, H. P. (2018). A macro-element for integrated time domain analyses representing bucket foundations for offshore wind turbines. Marine Structures, 59, 1-25.

Sørensen, S. P. H., & Ibsen, L. B. (2013). Assessment of foundation design for offshore monopiles unprotected against scour. *Ocean Engineering*, *63*, 17-25.

Tseng, W. C., Kuo, Y. S., Lu, K. C., Chen, J. W., Chung, C. F., & Chen, R. C. (2018). Effect of scour on the natural frequency responses of the meteorological mast in the taiwan strait. *Energies*, *11*(4), 823.

Van der Tempel, J., & Molenaar, D. P. (2002). Wind turbine structural dynamics–a review of the principles for modern power generation, onshore and offshore. *Wind engineering*, *26*(4), 211-222.

Van der Tempel, J., Zaaijer, M. B., & Subroto, H. (2004). The effects of Scour on the design of Offshore Wind Turbines. In *Proceedings of MAREC*. https://ocw.tudelft.nl/wp-content/uploads/Scour___MAREC_2004.pdf

Veletsos, A. S., & Meek, J. W. (1974). Dynamic behavior of building-foundation systems. *Earthquake Engineering & Structural Dynamics*, 3(2), 121-138.

Weijtjens, W., Verbelen, T., De Sitter, G., & Devriendt, C. (2016). Foundation structural health monitoring of an offshore wind turbine—a full-scale case study. *Structural Health Monitoring*, *15*(4), 389-402.

Weijtjens, W., Verbelen, T., Capello, E., & Devriendt, C. (2017). Vibration based structural health monitoring of the substructures of five offshore wind turbines. *Procedia engineering*, *199*, 2294-2299.

Zaaijer, M. B., & Van der Tempel, J. (2004). Scour protection: a necessity or a waste of money. In *Proceedings of the 43 IEA Topixal Expert Meeting* (pp. 43-51).

Zaaijer, M. B. (2006). Foundation modelling to assess dynamic behaviour of offshore wind turbines. *Applied Ocean Research*, *28*(1), 45-57.